ACADEMIC PRESS

Available online at www.sciencedirect.com

SCIENCE DIRECT®

Journal of Solid State Chemistry 170 (2003) 247–254

JOURNAL OF SOLID STATE CHEMISTRY

http://elsevier.com/locate/jssc

A TEM, XRD, and crystal chemical investigation of oxygen/vacancy ordering in $(Ba_{1-x}La_x)_2In_2O_{5+x}$, $0 \leqslant x \leqslant 0.6$

Yun Liu,[a] Ray L. Withers,[a,*] and John Fitz Gerald[b]

[a] *Research School of Chemistry, Australian National University, GPO Box 4, Canberra ACT 0200, Australia*
[b] *Research School of Earth Sciences, Australian National University, Canberra ACT 0200, Australia*

Received 4 June 2002; received in revised form 12 September 2002; accepted 7 October 2002

Abstract

A careful TEM and XRD study of the $(Ba_{1-x}La_x)_2In_2O_{5+x}$, $0 \leqslant x \leqslant 0.6$, 'defect-perovskite'-type solid solution has been carried out. A well-defined structural phase transition is shown to occur between $x = 0.1$ and 0.2 from the orthorhombic brownmillerite structure type on the low x side to a multiple twinned, tetragonal $1 \times 1 \times 2$ perovskite-related superstructure phase on the high x side at $x = 0.2$. This phase transition correlates with an important phase transition previously observed in electrical conductivity versus temperature measurements. The existence of additional satellite reflections close to the $\mathbf{G} \pm \frac{1}{2} \langle 001 \rangle_p^*$ regions of reciprocal space was found to be typical of all $(Ba_{1-x}La_x)_2In_2O_{5+x}$ specimens, although their intensity relative to the parent Bragg reflections systematically reduces as x increases. As x increases beyond 0.2, the $\mathbf{G} \pm \frac{1}{2} \langle 001 \rangle_p^*$-type satellite reflections initially become weaker and rather more diffuse for $x = 0.3$ before splitting into pairs of rather weak and somewhat diffuse incommensurate satellite reflections for $x = 0.4$ and beyond. An interpretation in terms of oxygen vacancy ordering and associated structural relaxation is given. Additional structured diffuse scattering is also observed and a tentative explanation in terms of Ba/La ordering and associated local strain distortions put forward.
© 2002 Elsevier Science (USA). All rights reserved.

Keywords: $(Ba_{1-x}La_x)_2In_2O_{5+x}$; Defect perovskite solid solution; Phase transition; TEM study; Structured diffuse scattering; Oxygen vacancy ordering

1. Introduction

The search for materials which exhibit fast oxygen ion conduction at the lowest possible temperatures (for use in a wide range of high-temperature electrochemical devices including oxygen gas sensors, solid oxide fuel cells, separation membranes, etc.) has recently focussed attention on oxides with the brownmillerite structure type [1–10]. The orthorhombic brownmillerite structure type of general stoichiometry $A_2B_2O_5$ can be described as an oxygen-vacancy-ordered "defect perovskite" in which one-sixth of the oxygen ions of the perovskite structure type are replaced by an ordered array of vacancies, producing alternating octahedrally and tetrahedrally co-ordinated B layers (see Fig. 1b). Perhaps not surprisingly, heating of brownmillerite-type oxides above a certain critical temperature often disorders these oxygen vacancies and results in fast oxygen ion conduction.

There has been much recent interest in $Ba_2In_2O_5$, in particular, as a result of the fact that above a phase transition at $\sim 925°C$ (prominent in Arrhenius $\log(\sigma) \alpha (1/T)$ plots, σ = conductivity, T = temperature) it has a high oxygen-ion conductivity comparable to that of yttria-stabilized zirconia, the most widely used oxygen-ion conductor [1–10]. Various authors have reported this as a direct orthorhombic brownmillerite to cubic "defect perovskite" phase transition [1,3]. Other authors [2,4], however, have suggested that this transition is a two-stage process with the first stage, $\sim 925°C$ phase transition representing a two-dimensional order–disorder phase transition (involving only the equatorial oxygen atoms within the tetrahedral layers of Fig. 1b) from an orthorhombic brownmillerite to an intermediate, also orthorhombic, layered structure type prior to a final transition to a cubic "defect perovskite" phase at $\sim 1075°C$. Still other authors [10] have found that the

*Corresponding author. Fax: +26-12-507-50.
E-mail address: withers@rsc.anu.edu.au (R.L. Withers).

0022-4596/03/$ - see front matter © 2002 Elsevier Science (USA). All rights reserved.
doi:10.1016/S0022-4596(02)00115-9

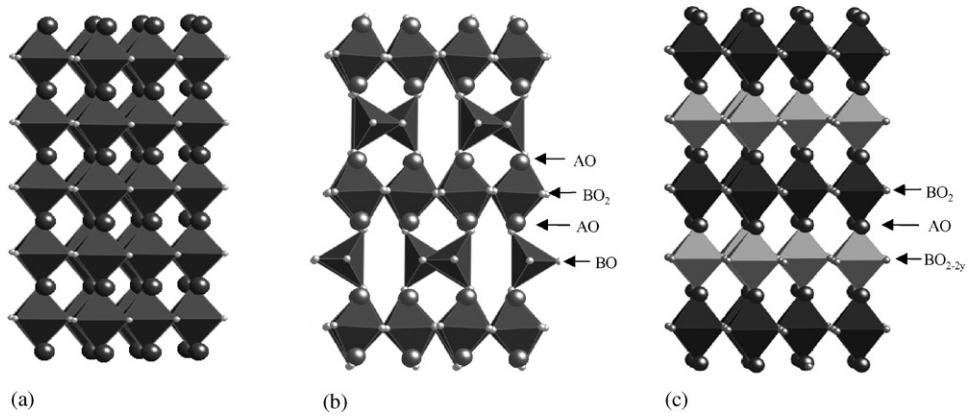

Fig. 1. Close to $\langle 110 \rangle_p$ projections of the (a) ideal cubic (*Pm3m* ABO_3 perovskite parent structure type, (b) the orthorhombic (*Ibm2*) $A_2B_2O_5$ brownmillerite structure type projected along its [001] direction (**a** horizontal and **b** vertical), and (c) the proposed $1 \times 1 \times 2$ tetragonal (*P4/mmm*) "defect perovskite" superstructure phase (projected very close to one of its $\langle 1\,1\,0 \rangle$ directions with **c** vertical). The BO_6 octahedra are shown dark while the oxygen-deficient BO_4 and BO_{6-2y} polyhedra of (b) and (c) are shown in grey. The A cations are represented by the large grey balls.

orthorhombic brownmillerite and cubic "defect perovskite" phases co-exist over a narrow temperature range and disputed the existence of an intermediate phase.

The desire to stabilize the high oxygen ion conducting polymorph/s has led to a variety of dopant schemes designed to lower or even suppress altogether the high-temperature phase transition/s [5–10]. In this paper, we focus on a dopant scheme involving the replacement of Ba ions with La ions leading to a coupled substitution of oxygen for vacancies and an overall stoichiometry $(Ba_{1-x}La_x)_2In_2O_{5+x}$ [6–9,11]. The resultant $(Ba_{1-x}La_x)_2In_2O_{5+x}$, $0 \leqslant x \leqslant 0.6$, phase field has been reported as a wide-range non-stoichiometric, "defect-perovskite"-type phase field. The underlying average structure at all compositions is the cubic *Pm3m* "defect perovskite" structure type (see Fig. 1a) while the $x = 0$ end member, $Ba_2In_2O_5$, is an oxygen-vacancy-ordered variant of this "defect perovskite" parent of orthorhombic brownmillerite structure type (see Fig. 1b).

Both Kakinuma et al. [6,7] and Uchimoto et al. [8,9] have shown that increasing La content systematically suppresses the high-temperature phase transition (apparent in $\log(\sigma)\alpha(1/T)$ plots for low x) until it disappears altogether somewhere between $x = 0.1$ and 0.2 (at $x = 0.12$ according to Kakinuma et al. [7]). They also showed that oxide ion conductivity systematically increases with increasing La content. Despite their good agreement as regards conductivity versus composition measurements, Uchimoto et al. [8,9] and Kakinuma et al. [6,7] nonetheless report quite different crystallography versus composition results.

Uchimoto et al. [8,9], for example, detected no additional satellite reflections nor any splitting of the parent perovskite-type Bragg reflections in XRD patterns recorded at room temperature [8] for $x = 0.20$, 0.30, 0.40 or 0.50 and hence reported that $(Ba_{1-x}La_x)_2In_2O_{5+x}$ ($x = 0.2-0.5$) has the disordered cubic "defect perovskite" structure type (space group *Pm3m*). Kakinuma et al. [6], by contrast (and also from XRD data), reported three different crystal symmetries as a function of composition: orthorhombic ($0.0 \leqslant x \leqslant 0.3$), tetragonal ($0.3 \leqslant x \leqslant 0.5$) and cubic ($0.5 \leqslant x \leqslant 0.6$). Kakinuma et al. [6] "postulated that the reason why the crystal symmetry of the $(Ba_{1-x}La_x)_2In_2O_{5+x}$ system was not cubic in the composition range from $x = 0.2$ to 0.5 might depend on the two-dimensional migration of the oxygen ions" as discussed above in the context of the ~925°C phase transition of $Ba_2In_2O_5$ [2].

Even more recently, Mitome et al. [11] carried out a transmission electron microscopy (TEM) investigation of this system. It was reported that $(Ba_{1-x}La_x)_2In_2O_{5+x}$, $x = 0.1$, had a multiply twinned, ".. tetragonal brownmillerite structure with lattice parameters of $a = c = (\sqrt{2}/4)b = 0.59$ nm." As x increased beyond 0.1, they reported that the tetragonal brownmillerite domain size (of 30–50 nm in the case of $x = 0.1$) simply reduced in size until $x = 0.5$ when a domain structure could no longer be distinguished clearly. This was interpreted as the brownmillerite structure type reverting to the cubic "defect perovskite" structure type in the vicinity of $x = 0.5$. This, however, provides no explanation for the well-defined phase transition observed between $x = 0.1$ and 0.2 in the electrical conductivity versus temperature measurements [6–9].

Given these various discrepancies and the known ability of electron diffraction to reveal weak features of reciprocal space often undetected by means of XRD, a combined TEM and XRD investigation of the $(Ba_{1-x}La_x)_2In_2O_{5+x}$ system was undertaken with the specific purpose of searching for evidence of oxygen vacancy (and/or Ba/La) ordering and associated

structural relaxation. It was hoped to thereby obtain a structural explanation for the well-defined phase transition observed between $x = 0.1$ and 0.2 in electrical conductivity versus temperature measurements [6–9].

2. Synthesis and data collection

The $(Ba_{1-x}La_x)_2In_2O_{5+x}$ ($0 \leqslant x \leqslant 0.6$) specimens, used in this study, were prepared by conventional solid-state reaction starting from barium carbonate ($BaCO_3$, 5 N, Alfa), indium oxide (In_2O_3, 4 N, Aldrich) and lanthanum oxide (La_2O_3, 4 N, Selbys). The raw materials were initially dried at 120°C for a week to remove any adsorbed water. Seven samples in the desired composition range (at $x = 0$, 0.1, 0.2, 0.3, 0.4, 0.5 and 0.6) were made by adding stoichiometric amounts of the reactants and thoroughly grinding together in a mortar. The mixtures were then heat-treated at 1000°C for 24 h in order for decarbonation to take place. The resultant powders were then ground again, pressed to pellets and sintered at 1300°C for a further 48 h before quenching in air. The outer surface layer of the resultant pellets was polished off before grinding and subsequent examination.

The products were examined by X-ray powder diffraction (XRPD), using the Guinier–Hägg camera technique with monochromatized Cu$K\alpha$1 radiation. Silicon (NBS No.640) was added as an internal standard for accurate determination of the unit cell dimensions. XRD data confirmed the end products were phase pure $(Ba_{1-x}La_x)_2In_2O_{5+x}$ except for the $x = 0.6$ specimen in which traces of $LaInO_3$ and In_2O_3 could be detected. Samples suitable for TEM work were prepared by the dispersion of finely ground material onto a holey carbon film. TEM work was carried out using Philips EM 430 and CM 30 TEMs.

3. XRD results

The XRD patterns of $Ba_2In_2O_5$ ($x = 0$) and $(Ba_{1-x}La_x)_2In_2O_{5+x}$ ($x = 0.1$) at room temperature were both indexed to body-centred orthorhombic unit cells ($a = 6.100(1)$ Å, $b = 16.723(3)$ Å, and $c = 5.961(1)$ Å in the case of $Ba_2In_2O_5$; $a = 6.051(3)$ Å, $b = 16.754(7)$ Å, and $c = 5.931(3)$ Å in the case of $(Ba_{1-x}La_x)_2In_2O_{5+x}$, $x = 0.1$). The refined $Ba_2In_2O_5$ lattice parameters are in good agreement with previously reported values for $Ba_2In_2O_5$. The extinction conditions were consistent with the usual space group symmetry reported for orthorhombic brownmillerite phases (in this setting) of *Ibm*2 or *Ibmm*.

Upon increasing x, the underlying volume of the "defect-perovskite"-type average structure unit cell systematically shrank (see Table 1) due to the smaller size of the dopant La^{3+} ion. For the $x \geqslant 0.2$ specimens, no splitting of the cubic perovskite parent Bragg reflections could be detected in agreement with the observations by Uchimoto et al. [6]. In the case of the $x = 0.2$ specimen, a few, very weak additional satellite reflections (requiring a doubling of at least one of the parent perovskite unit cell dimensions) were detected and subsequently confirmed by electron diffraction (see below). The refined unit cell dimensions are given in Table 1 and are in good agreement with those previously reported for $x = 0.2$ and 0.4 by Uchimoto et al. [8] (ignoring the cell doubling detected in the present paper for $x = 0.2$) but not with those reported by Kakinuma et al. [6]. We did not find any trace of the intermediate metrically tetragonal phase reported by Kakinuma et al. [6].

Table 1
Refined lattice parameters (Å) of $(Ba_{1-x}La_x)_2In_2O_{5+x}$

x	a	b	c
0	6.100(1)	16.723(3)	5.961(1)
0.1	6.051(3)	16.754(7)	5.931(3)
0.2	4.203(2)	8.406(3)	4.203(2)
0.3	4.1680(5)		
0.4	4.1640(6)		
0.5	4.1586(5)		
~0.6	4.1553(6)		

4. TEM results

Electron diffraction investigation of the reciprocal lattices of the various $(Ba_{1-x}La_x)_2In_2O_{5+x}$ specimens showed a complex mixture of diffraction features in addition to the strong underlying parent (subscript p in what follows) reflections of the cubic "defect perovskite" average structure (hereafter labelled G). The reciprocal lattice of the brownmillerite structure type (*Ibm*2, $\mathbf{a} = \mathbf{a}_p - \mathbf{c}_p$, $\mathbf{b} = 4\mathbf{b}_p$, $\mathbf{c} = \mathbf{a}_p + \mathbf{c}_p$; $\mathbf{a}^* = \frac{1}{2}[10\bar{1}]_p*$, $\mathbf{b}^* = \frac{1}{4}[010]_p*$, $\mathbf{c}^* = \frac{1}{2} : [101]_p*$, for example, is necessarily characterized by the existence of both $\mathbf{G} \pm \frac{1}{4}[21\bar{2}]_p*$ as well as $\mathbf{G} \pm \frac{1}{2}[010]_p*$ satellite reflections. In the case of the $x = 0$ and 0.1 specimens, both types of satellite reflections are indeed present (see, for example, the $[001] \equiv [101]_p$ zone axis EDP of the $x = 0.1$ specimen shown in Fig. 2a). In the case of the $x \geqslant 0.2$ specimens, however, the former $\mathbf{G} \pm \frac{1}{4}[21\bar{2}]_p^*$ satellite reflections have disappeared (cf. Fig. 2a with Fig. 2b) i.e., there exists a well-defined change in structure type between $x = 0.1$ and 0.2 which correlates both with the above XRD results as well as with the well-defined phase transition observed between $x = 0.1$ and 0.2 in electrical conductivity versus temperature measurements [6–9]. This phase transition, however, is not a direct brownmillerite to cubic "defect perovskite" phase transition (see, for

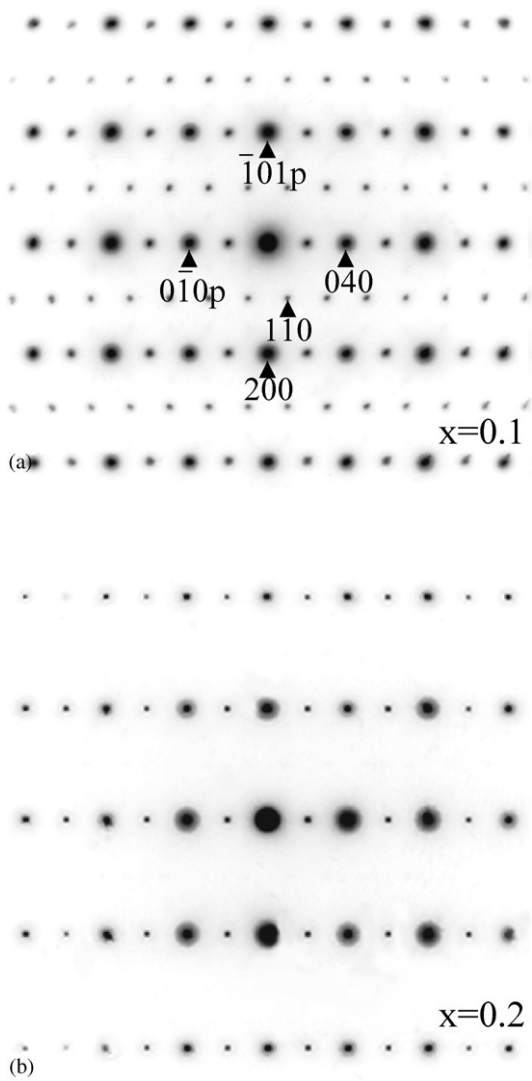

Fig. 2. Shows (a) an $[001] \equiv [101]_p$ zone axis EDP of the *Ibm*2 brownmillerite structure type at $x = 0.1$ (indexation is given both with respect to the underlying defect perovskite parent structure, subscript p, as well as with respect to the actual brownmillerite cell) and (b) a corresponding $\langle 101 \rangle_p$ zone axis EDP of the *P*4/*mmm* "defect perovskite" superstructure phase at $x = 0.2$. Note that the $\mathbf{G} \pm \frac{1}{2}[21\bar{2}]_p^*$-type satellite reflections (such as that indexed as 1 1 0 in (a)) have disappeared in (b) (cf. Fig. 2a with Fig. 2b) i.e., there exists a well-defined change in structure type between $x = 0.1$ and 0.2.

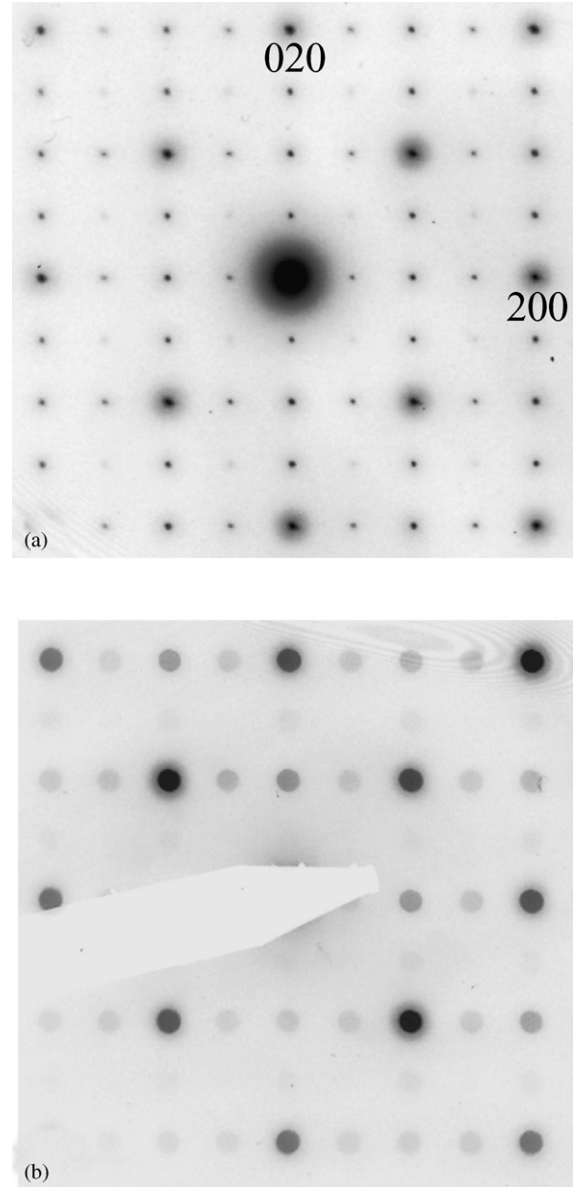

Fig. 3. Shows (a) a typical $\langle 001 \rangle_p$-type selected area EDP of the $x = 0.2$ specimen along with (b) a corresponding $\langle 001 \rangle_p$-type micro-diffraction taken from a much smaller area. Note the absence of the $\mathbf{G} \pm \frac{1}{2}[001]_p^*$ satellite reflections in the latter.

example, Ref. [11]) as the $\mathbf{G} \pm \frac{1}{2}\langle 010 \rangle_p^*$-type satellite reflections remain, although weakened, for the $x = 0.2$ specimen (see Fig. 2b).

The existence of additional satellite reflections close to the $\mathbf{G} \pm \frac{1}{2}\langle 010 \rangle_p^*$ regions of reciprocal space was found to be typical of all $(Ba_{1-x}La_x)_2In_2O_{5+x}$ specimens, although their intensity relative to the parent Bragg reflections systematically reduces as x increases. No other types of satellite reflections were ever observed for the $x \geqslant 0.2$ specimens. In the case of the $x = 0.2$ specimen, these additional satellite reflections were quite sharp as well as relatively strong, consistent with their being weakly detected in XRD traces as discussed above. A typical $\langle 001 \rangle_p$-type selected area EDP is shown in Fig. 3a. The virtual absence of $\mathbf{G} \pm \frac{1}{2}\langle 110 \rangle_p^*$-type satellite reflections in this EDP is suggestive that the local symmetry may well be lower than cubic and that the simultaneous presence of $\mathbf{G} \pm \frac{1}{2}\langle 100 \rangle_p^*$ and $\mathbf{G} \pm \frac{1}{2}\langle 010 \rangle_p^*$ reflections in Fig. 3a may be a result of twinning. That the local symmetry is indeed not cubic, despite the metric cubic symmetry found from XRD, is clear from the $\langle 001 \rangle$-type micro-diffraction pattern shown in Fig. 3b and the typical $\langle 001 \rangle$ lattice image shown in Fig. 4, revealing shapeless domains ca 10 nm in diameter. A similar lattice image of the $x = 0.2$ material

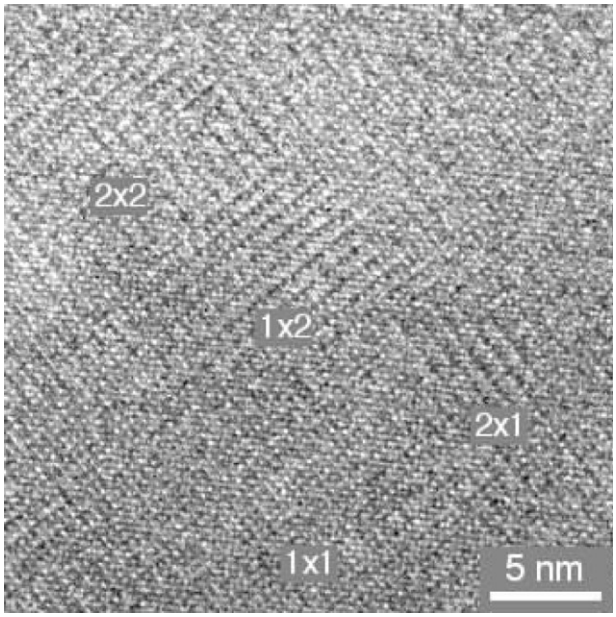

Fig. 4. [001] lattice image typical of the $x = 0.2$ material. Doubled {100} fringes define a domain micro-structure on the 10 nm scale. Examples of four different regions are labelled: 1×1 has no doubling of fringes, 2×2 has doubled fringes in both directions, 1×2 and 2×1 have just one direction of doubling.

was published as Fig. 5 of Ref. [11]. It was interpreted therein, however, as micro-twinned domains of brown-millerite-structured material.

The presence of a micro-domain texture is immediately apparent in such $\langle 001 \rangle$ lattice images (see Fig. 4). Regions showing doubling along [100] but not [010] or vice versa, i.e., 2×1 as well as 1×2 regions, are quite common as are regions where such fringes appear to terminate. 1×1 and 2×2 regions are also apparent, the existence of the former implying the $1 \times 1 \times 2$ super-lattice model is the correct one. In this case, the existence of the 2×2 regions can be interpreted as arising from overlapping 2×1 and 1×2 domain regions along the incident beam direction. 1×1 regions should, however, never occur if the $2 \times 2 \times 1$ model is correct. It is, however, difficult to definitively rule out the $2 \times 2 \times 1$ model as the probability of overlapping domains along the incident beam direction often leads to a weak hint of doubling along one or other direction.

As x increases beyond 0.2, the $\mathbf{G} \pm \frac{1}{2} \langle 001 \rangle_p^*$-type satellite reflections initially become weaker and rather more diffuse for $x = 0.3$ consistent with Mitome et al.'s [11] explanation in terms of decreasing domain size with increasing x (cf. the typical close to $\langle 001 \rangle$-type EDP for $x = 0.3$ shown in Fig. 5a with Fig. 3a) before splitting into pairs of rather weak and somewhat diffuse incommensurate satellite reflections for $x = 0.4$ and beyond (see, for example, the typical $\langle 001 \rangle$-type EDP for $x = 0.4$ shown in Fig. 5b). Note that the incommensurate satellite reflections at $x = 0.4$, while somewhat

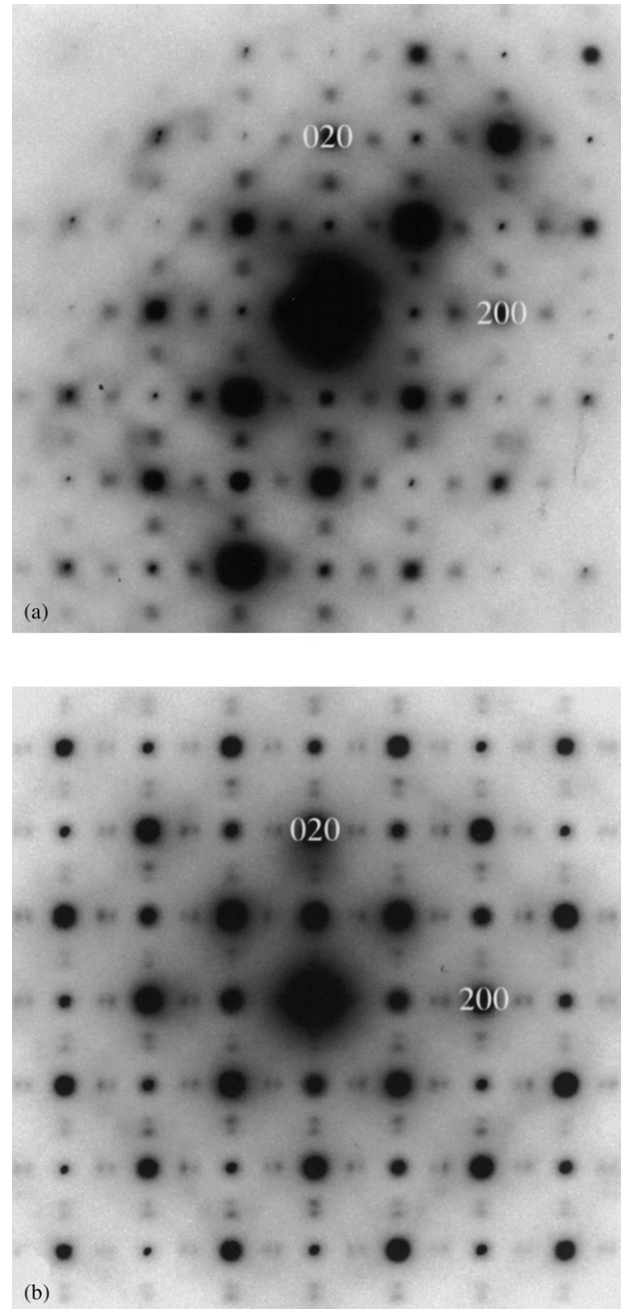

Fig. 5. Shows (a) a typical close to $\langle 001 \rangle$-type selected area EDP for $x = 0.3$ and (b) the corresponding $\langle 001 \rangle$-type EDP for $x = 0.4$. Note that the the very diffuse $\mathbf{G} \pm \frac{1}{2} \langle 001 \rangle_p^*$-type satellite reflections of (a) have split into pairs of somewhat sharper incommensurate satellite reflections for $x = 0.4$.

diffuse, are nonetheless sharper than the $\mathbf{G} \pm \frac{1}{2} \langle 001 \rangle_p^*$-type satellite reflections at $x = 0.3$ (cf. Fig. 5b with Fig. 5a) implying a longer real space correlation length or larger domain size. The magnitude of the incommensurate primary modulation wave vector is ~ 0.43 at $x = 0.4$ and does not appear to change with further increase in x. The weakness of these satellite reflections in reciprocal space is reflected in the virtual absence of any

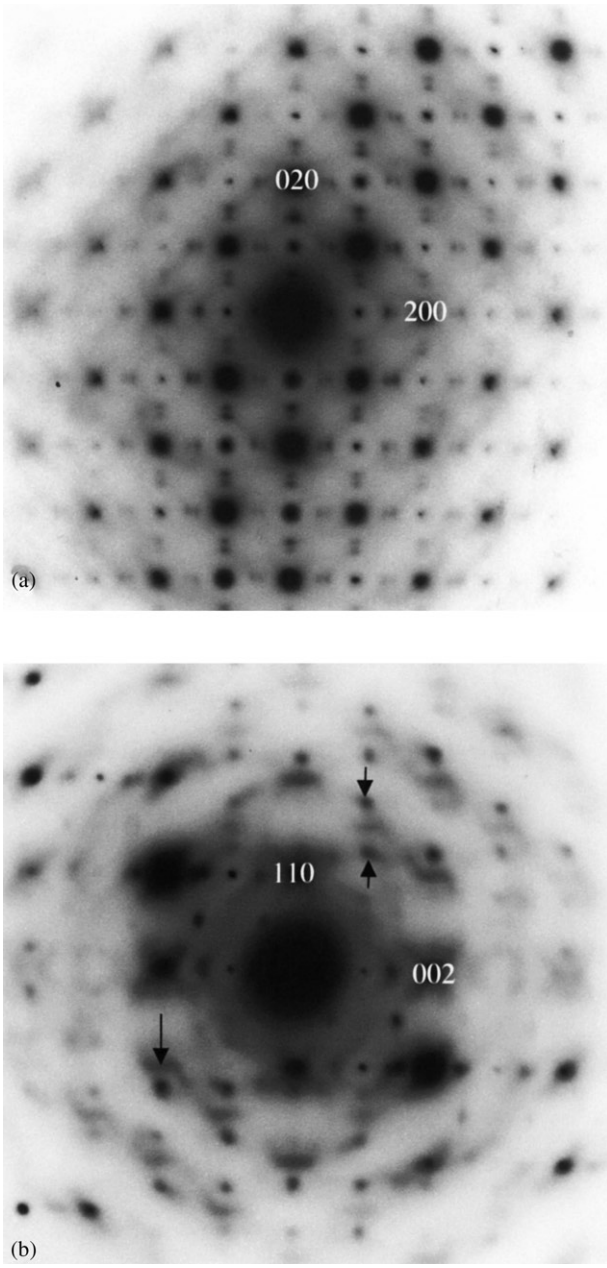

Fig. 6. Shows (a) a close to $\langle 001 \rangle$ zone axis EDP for the $x = 0.4$ specimen in which a fascinating and characteristic banded diffuse distribution running through the incommensurate satellite reflections along the $\langle 110 \rangle^*$ directions of reciprocal space is apparent. (b) shows an over-exposed EDP of an $x = 0.5$ specimen obtained by tilting $\sim$6–7° away from a $\langle \bar{1}10 \rangle$ zone axis orientation keeping the $[11\bar{2}]*$ reflection excited. Note the polarized diffuse banding once more this time running along the $\langle 112 \rangle^*$ directions of reciprocal space, but again through the satellite reflections. In both cases, note that diffuse intensity is systematically transferred from light 'bands' in reciprocal space centred on parent Bragg reflections for which $h+k+l$ is odd to dark 'bands' centred on parent Bragg reflections for which $h+k+l$ is even.

superlattice contrast in corresponding $\langle 001 \rangle$-type lattice images or their Fourier transforms. The only feature apparent in such images is that, over lengths ca 10 nm, strings of higher or lower image intensity run along one or the other $\langle 100 \rangle_p$ directions, but appear to lack correlation across the image.

In addition to the satellite reflections in the vicinity of the $\mathbf{G} \pm \frac{1}{2} \langle 001 \rangle_p^*$ regions of reciprocal space, rather more complicated structured diffuse scattering is also apparent in all $x \geqslant 0.2$ specimens, particularly upon tilting slightly away from exact zone axis orientations and exposing the corresponding EDPs for a sufficiently long time. Fig. 6a, for example, shows a close to $\langle 001 \rangle$ zone axis EDP for the $x = 0.4$ specimen in which a fascinating and characteristic banded diffuse distribution running through the incommensurate satellite reflections along the $\langle 110 \rangle^*$ directions of reciprocal space is apparent. Diffuse intensity is systematically transferred from light 'bands' in reciprocal space centred on parent Bragg reflections for which $h+k+l$ is odd to dark 'bands' centred on parent Bragg reflections for which $h+k+l$ is even. Note that these diffuse bands are polarized (i.e., most visible along directions of reciprocal space perpendicular to the direction of the banding itself, implying that the diffuse is arising from displacements also perpendicular to the direction of the banding itself) and that the edges of the bands appear to run through the satellite reflections.

This characteristic 'banding' is always present (for all $x \geqslant 0.2$ specimens) although not necessarily always as prominently as in Fig. 6a. Fig. 6b, for example, shows an over-exposed EDP of an $x = 0.5$ specimen obtained by tilting $\sim$6–7° away from a $\langle \bar{1}10 \rangle$ zone axis orientation keeping the $[11\bar{2}]*$ reflection excited. Note the polarized diffuse banding once more this time running along the $\langle 112 \rangle^*$ directions of reciprocal space, but again through the satellite reflections. The two arrowed apparent superlattice reflections on either side of one such diffuse dark band in the upper right quadrant of Fig. 6b, for example, can be indexed as $[111]^* + \sim\frac{1}{2}\mathbf{b}^*$ and $[221]* - \sim\frac{1}{2}\mathbf{a}^*$ satellite reflections, respectively. Figs. 6a and b taken together suggest that, in reciprocal space, planes of diffuse intensity occur perpendicular to all parent $\langle 111 \rangle$ directions and thus form octahedral shapes in reciprocal space. One consequence of this is that EDPs for $\langle 111 \rangle_p$ zone axes show no trace of the diffuse banding, even when heavily exposed. Finally note the sharper, more or less continuous structured diffuse scattering which occurs within the overall diffuse banding (arrowed in the bottom left of Fig. 6b). This more or less continuous structured diffuse scattering is present for all $x \geqslant 0.2$ specimens.

5. Interpretation

The existence of additional satellite reflections at the $\mathbf{G} \pm \frac{1}{2} \langle 001 \rangle_p^*$ regions of reciprocal space in conjunction with the experimental evidence for twinning described

above suggests the presence of a multiply twinned $1\times1\times2$ or $2\times2\times1$ (most likely $1\times1\times2$) tetragonal "defect perovskite" superlattice phase in the case of the $x=0.2$ specimen. A $2\times2\times1$ tetragonal "defect-perovskite"-type superlattice has been reported previously in the case of the oxygen-deficient "defect perovskites" $SrTi_{0.4}Fe_{0.6}O_{2.70}$ and $SrTi_{0.2}Fe_{0.8}O_{2.60}$ [12]. It was not clear, however, in this case whether the possibility of a twinned $1\times1\times2$ explanation was even considered let alone ruled out. Furthermore, no plausible structural model or explanation for the reported superlattice was put forward. By contrast, well-characterized tetragonal $1\times1\times2$ phases (space group $P4/mmm$) have recently been reported for two "defect perovskites", $Sr_2MnGaO_{5.47}$ [13] and $LaSrCuGaO_{5-\delta}F_{2\delta}$ [14]. Intriguingly, these recent examples have been shown to evolve from original brownmillerite-type phases upon oxidation in the case of $Sr_2MnGaO_{5.47}$ [13] and upon fluorination in the case of $LaSrCuGaO_{5-\delta}F_{2\delta}$ [14].

The plausible explanation for the observed $1\times1\times2$ superstructures given in these latter two cases is that the necessary addition of further anions into the equatorial BO layers of Fig. 1b leads to a two-dimensional disordering of the anions within these layers and a resultant $P4/mmm$, $1\times1\times2$ tetragonal superstructure resulting from the alternation of filled and partially filled equatorial layers (see Fig. 1c). Such a mechanism also seems the most plausible explanation for the observed satellite reflections in the current case as well as being compatible with the observed diffraction evidence (see Fig. 2b and 3b). It is reminiscent of the two-dimensional order–disorder phase transition mechanism put forward for $Ba_2In_2O_5$ itself [2]. The observed systematic decrease in intensity of the satellite reflections as x increases is then only to be expected as the difference in vacancy concentration between the filled and partially filled equatorial layers systematically diminishes.

The existence of incommensurate satellite reflections for $x\geqslant0.4$ may indicate a disruption of the doubled …OTOT… (i.e., filled, partially filled, filled, partially filled) layer stacking sequence (see Fig. 1c) caused by the introduction of some …OO… sequences. Some justification for this assumption can be obtained from the existence of ordered defect perovskites such as $Ca_2LaFe_3O_8$ [15] with a stacking sequence of …OOTOOT… and $Ca_4YFe_5O_{13}$ [16] with the stacking sequence …OTOOTOTOOTO… [11]. It is interesting to note in these latter cases that the three-valent ion in the nominally perovskite A site is always situated between the octahedral …OO… layers, thus avoiding nearest-neighbour oxygen vacancy sites. Bond valence sum calculations (see Table 2) can be used to provide some indirect justification for such an assertion. Table 2, for example, shows bond valence sums (or apparent valences (AVs) [17]) of the various In, Ba, La and O ions calculated using two different models—the ideal

Table 2
Bond valence sums for $(Ba_{1-x}La_x)_2In_2O_{5+x}$, $x=0.2$ ($a_p=4.203$ Å)

	AV (In)	AV (Ba)	AV (La)	AV (O)
Ideal perovskite parent model	2.33 (4)	1.58 (10)	1.15 (10)	
$a=4.203$ Å	2.92 (5)	1.74 (11)	1.27 (11)	1.77
	3.50 (6)	1.90 (12)	1.38 (12)	
	2.69 (4)			
$P4/mmm$ model ($\varepsilon=0.1$ Å)	3.28 (5)	1.58 (10)	1.15 (10)	1.77
$a=b=4.203$ Å, $c=8.406$ Å	3.86 (6)	1.74 (11)	1.26 (11)	1.81
		1.90 (12)	1.38 (12	1.77
	3.22 (6)			
Ideal valence sum	3.00	2.00	3.000	2.000

The number in brackets represents the co-ordination number (n).
In the $P4/mmm$ model, the apical oxygens move ε Å away from the fully occupied equatorial O layer and towards the partially occupied equatorial O layer.

$Pm3m$, defect perovskite parent model and the $P4/mmm$, $1\times1\times2$ model. The fractional co-ordinates (used to calculate the AVs of Table 2) in the former model are well known while those for the latter model (In1 at 0 0 0, In2 at $0,0,\frac{1}{2}$; (Ba,La) at $\frac{1}{2},\frac{1}{2},\frac{1}{4}+\varepsilon_A$; O1 at $\frac{1}{2},0,\frac{1}{2}$; O2 at $0,0,\frac{1}{4}-\varepsilon_O$ and O3 at $\frac{1}{2},0,0$; $a=b=4.2030$ Å, $c=8.4060$ Å) were derived using Table 4 of Ref. [13].

In the latter model, the apical O2 oxygens between the partially occupied and fully occupied equatorial oxygen layers are allowed by $P4/mmm$ symmetry to move along **c** away from the fully occupied equatorial oxygen layers towards the partially occupied equatorial oxygen layers to compensate for the respective under- and over-bonding of the 4- and 6-co-ordinate In ions (Ins 1 and 2, respectively) in the ideal defect perovskite parent model (see Table 2). The magnitude of this parameter, ε_O, was chosen such that $\varepsilon_O c=0.1$ Å for the purposes of calculating the AVs in Table 2. (Note that $P4/mmm$ symmetry also allows the Ba/La ions to displace along **c** but this was found not to improve the local crystal chemistry and so this parameter, ε_A, was put to zero for the purposes of calculating AVs in Table 2.) The parent cell parameter used for both models was that appropriate for $x=0.2$ i.e., 4.203 Å (see Table 1). Note that for $x=0.2$, and assuming an (unlikely) random distribution of oxygen vacancies within the partially occupied tetrahedral layers, the probability that the 'tetrahedrally' co-ordinated In1 is surrounded by four O's is 64%, surrounded by five O's is 32% or surrounded by six O's is 4%. The AVs of In1 for each of these three cases are listed together in the column labelled AV(In) in Table 2 while that appropriate to the 6-fold co-ordinated In2 is listed below these values after a line break. Likewise, the probability that the Ba/La ion is surrounded by 10 O's is 64%, surrounded by 11 O's is 32% or surrounded by 12 O's is 4%. The AVs for each of these cases are also listed in Table 2 along with the AVs of O1, O2 and O3.

For the ideal defect perovskite parent model, it can be seen that the In ions would be happiest with 5-fold co-ordination rather than 4 or 6 while the Ba ions would be slightly, but not that significantly, under-bonded if 10- or 11-fold co-ordinated and relatively happily bonded if 12-fold co-ordinated. The La ions, by contrast, are very significantly under-bonded whether 10-, 11- or 12-fold co-ordinated. Clearly the last thing a La ion needs is an oxygen vacancy in its nearest neighbour shell of surrounding oxygen ions. For this to be avoided, however, a disruption to the normal …OTOT… layer stacking sequence via the introduction of some …OO… sequences as discussed above is needed.

The relaxation of the apical oxygen ions along **c** in the $P4/mmm$ model can clearly simultaneously and significantly improve the local crystal chemistry of both the 'tetrahedrally' co-ordinated (In1) and octahedrally co-ordinated (In2) In ions (see Table 2). It has very little effect, however, upon the local crystal chemistry of the heavily under-bonded La ions. This could only be improved by a very significant contraction in the local LaO_{12} co-ordination polyhedra or parent unit cell dimension. Insertion of more and more La ions upon increasing x can therefore be expected to lead to ever increasing local structural distortion and strain presumably giving rise to the additional structured diffuse scattering apparent for $x \geqslant 0.2$ (see Fig. 6).

The diffuse banding, i.e., the systematic transfer of diffuse intensity from light bands to dark 'bands' (see Fig. 6) is strongly reminiscent of the so-called atomic size effect (see, for example, Fig. 1 of Ref. [18]), usually thought of as arising from a coupling between compositional and displacive degrees of freedom in disordered systems [18–20]. The fact that the dark 'bands' are centred on parent Bragg reflections for which $h+k+l$ is even (see Fig. 6), requires that the correlated sites responsible are separated by $\Delta\mathbf{r}_{\mu\mu'} = \frac{1}{2}\langle 111 \rangle_{\mathrm{p}}$ in real space [19,21] while the fact that these diffuse bands are transverse polarized, i.e., most visible along directions of reciprocal space perpendicular to the direction of the banding itself, requires that the displacive shifts involved must primarily be along $\langle 111 \rangle_{\mathrm{p}}$ directions. The most plausible, although admittedly tentative, explanation is thus that the diffuse banding arises from a first-order size-effect-type relaxation (see Ref. [18]) along the local $\langle 111 \rangle_{\mathrm{p}}$ directions (associated with the Ba/La distribution on the parent perovskite A sites) whereby the A–'InO_6' distances (formally equal to $(\sqrt{3}/2)a_{\mathrm{p}}$) are reduced from the average value whenever the A site is occupied by a La ion (i.e., the local unit cell dimension shrinks thus shortening the La–O distances and improving the local crystal chemistry of the La ions) and increased to compensate whenever it is occupied by a Ba ion. Proof of this proposition, however, would require very significant real space Monte Carlo-type modelling well beyond the scope of the current contribution.

References

[1] J.B. Goodenough, J.E. Ruiz-Diaz, Y.S. Zhen, Solid State Ion. 44 (1990) 21–31.
[2] S.B. Adler, J.A. Reimer, J. Baltisberger, U. Werner, J. Am. Chem. Soc. 116 (1994) 675–681.
[3] G.B. Zhang, D.M. Smyth, Solid State Ion. 82 (1995) 161–172.
[4] C.A.J. Fisher, M.S. Islam, R.J. Brook, J. Solid State Chem. 128 (1997) 137–141.
[5] H. Yamamura, Y. Yamada, T. Mori, T. Atake, Solid State Ion. 108 (1998) 377–381.
[6] K. Kakinuma, H. Yamamura, H. Haneda, T. Atake, J. Therm. Anal. Cal. 57 (1999) 737–743.
[7] K. Kakinuma, H. Yamamura, H. Haneda, T. Atake, Solid State Ion. 140 (2001) 301–306.
[8] Y. Uchimoto, T. Yao, H. Takagi, T. Inagaki, H. Yoshida, Electrochemistry 68 (2000) 531–533.
[9] Y. Uchimoto, H. Takagi, T. Yao, N. Ozawa, T. Inagaki, H. Yoshida, J. Synchrotron Radiat. 8 (2001) 857–859.
[10] P. Berastagui, S. Hull, F.J. García-García, S.-G. Eriksson, J. Solid State Chem. 164 (2002) 119–130.
[11] M. Mitome, M. Okamoto, Y. Bando, H. Yamamura, J. Vac. Sci. Technol. B 19 (2001) 2284–2288.
[12] S. Steinsvik, R. Bugge, J. Gjønnes, J. Tafto, T. Norby, J. Phys. Chem. Solids 58 (1997) 969–976.
[13] A.M. Abakumov, M.G. Rozova, P.Ph. Pavlyuk, M.V. Lobanov, E.V. Antipov, O.I. Lebedev, G. van Tendeloo, O.L. Ignatchik, E.A. Ovtchenkov, Yu.A. Koksharov, A.N. Vasil'ev, J. Solid State Chem. 160 (2001) 353–361.
[14] J. Hadermann, G. van Tendeloo, A.M. Abakumov, B.Ph. Pavlyuk, M. Rozova, E.V. Antipov, Int. J. Inorg. Mater. 2 (2000) 493–502.
[15] J.C. Grenier, J. Darriet, M. Pouchard, P. Hagenmuller, Mater. Res. Bull. 11 (1976) 1219–1225.
[16] Y. Bando, Y. Sekikawa, H. Yamamura, Y. Matsui, Acta Crystallogr. A 37 (1981) 723–728.
[17] N.E. Brese, M. O'Keeffe, Acta Crystallogr. B 47 (1991) 192–197.
[18] T.R. Welberry, J. Appl. Crystallogr. 19 (1986) 382–389.
[19] B.D. Butler, R.L. Withers, T.R. Welberry, Acta Crystallogr. A 48 (1992) 737–746.
[20] A.-K. Larsson, R.L. Withers, L. Stenberg, J. Solid State Chem. 127 (1996) 222–230.
[21] R.L. Withers, Th. Proffen, T.R. Welberry, Phil. Mag. A 79 (1999) 753–762.